Title	Selective laser sintering of hydroxyapatite/poly-epsilon-caprolactone scaffolds
Author(s)	Lohfeld, Stefan
Publication Date	2010
Publication Information	Eosoly, S; Brabazon, D; Lohfeld, S; Looney, L (2010) 'Selective laser sintering of hydroxyapatite/poly-epsilon-caprolactone scaffolds'. Acta Biomaterialia, 6 :2511-2517.
Link to publisher's version	http://dx.doi.org/10.1016/j.actbio.2009.07.018
Item record	http://hdl.handle.net/10379/5353
DOI	http://dx.doi.org/DOI 10.1016/j.actbio.2009.07.018

Selective laser sintering of hydroxyapatite/poly-ε-caprolactone scaffolds

Szilvia Eosoly [a], Dermot Brabazon [a], Stefan Lohfeld [b], Lisa Looney [a]

a School of Mechanical and Manufacturing Engineering, Dublin City University, Collins Avenue Glasnevin, Dublin 9, Ireland

b National University of Ireland, Galway, Ireland

Abstract

Selective laser sintering (SLS) enables the fabrication of complex geometries with the intricate and controllable internal architecture required in the field of tissue engineering. In this study hydroxyapatite and poly-ε-caprolactone, considered suitable for hard tissue engineering purposes, were used in a weight ratio of 30:70. The quality of the fabricated parts is influenced by various process parameters. Among them Four parameters, namely laser fill power, outline laser power, scan spacing and part orientation, were identified as important. These parameters were investigated according to a central composite design and a model of the effects of these parameters on the accuracy and mechanical properties of the fabricated parts was developed. The dimensions of the fabricated parts were strongly dependent on the manufacturing direction and scan spacing. Repeatability analysis shows that the fabricated features can be well reproduced. However, there were deviations from the nominal dimensions, with the features being larger than those designed. The compressive modulus and yield strength of the fabricated microstructures with a designed relative density of 0.33 varied between 0.6 and 2.3 and 0.1 and 0.6 MPa, respectively. The mechanical behavior was strongly dependent on the manufacturing direction.

1. Introduction

Selective laser sintering (SLS) is an additive manufacturing technology where parts are constructed by the sequential and controlled deposition of powder in a layer by layer fashion. In each layer the powder surface is selectively scanned according to the cross-sectional data of a previously created three-dimensional (3D) computer-aided design model. In the scanned regions particle coalescence is associated with a significant reduction in surface energy, which is the main driving force of sintering [1]. SLS has the potential to fabricate complex geometries with intricate and controllable internal architectures, such as that required for tissue scaffolds. Scaffolds are porous 3D matrices with high surface to volume ratios to which cells can attach and on which they can differentiate.

SLS enables the processing of numerous biocompatible polymers available in the form of powders. Some groups were able to directly fabricate bioceramic bone implants using an experimental SLS system [2,3], however, to process bioceramics a thermoplastic polymer functioning as a binder material is usually required, as the lasers used in typical commercial SLS systems are unable to fuse ceramic particles together. Several biocompatible polymers have been used for SLS fabrication of scaffolds, including polyethylene, polyetheretherketone, polycaprolactone, polylactide glycolide, polyvinyl alcohol and their composites with hydroxyapatite and other bioceramics [4-12]. However, much of this research has only demonstrated the feasibility of fusing powder particles together, and not the fabrication of complex predesigned 3D structures. Studies which did produce complex predesigned 3D structures via SLS were those by Williams et al., Zhou et al. and Partee et al. [13-15]. Williams et al. fabricated cylindrical porous scaffolds with a 3D orthogonal periodic architecture using polycaprolactone with a designed pore size of 1.75 mm. Zhou et al. produced 3D scaffolds with rectangular channels using poly(L-lactide) and poly(L-lactide)/ carbonated hydroxyapatite (HA) microspheres. Partee et al. optimized selective laser sintering of polycaprolactone scaffolds using a 25 full factorial design. However, in many other investigations of SLS of biodegradable biomaterials for tissue engineering applications the process was examined using a "one at a time" approach to vary process parameters [2-10]. In fact, the mechanical proper-ties and accuracy of specimens obtained from SLS processing are a result of the interactive influences of the different process parameters. When a combination of several independent variables and their interactions affect the measured responses, response surface methodology (RSM) is an effective tool for investigating the manufacturing process [16]. In this technique a least squares model is fitted to the experimental data which relates the output variables to the input parameters.

The central composite design (CCD) technique is often used to implement the RSM [17]. Adequacy of a proposed model from this analysis can be checked using analysis of variance (ANOVA) and the response surface plots can be employed to study the system relationships and locate the optimum within the range of investigated variables. In the present work a CCD was used to develop models describing the dependence of accuracy and mechanical properties on process parameters in the three principle building directions.

The main parameters that can be changed in a Sinterstation 2500^{Plus} SLS system are part bed temperature, layer thickness, laser power (outline and fill) and scan spacing. Of these parameters part bed temperature and layer thickness were not examined in this study. The processing of PCL is sensitive to temperature but temperature control of the SLS system used is not precise enough to examine its effect within the temperature range suitable for the processing of PCL. The applicable layer thickness is largely dependent on the particle size and as the used particle size was in range of the sintering depth, this parameter was not altered. The effect of laser power and scan spacing on the density and mechanical properties of the parts has been extensively examined by others [10,12,18-22]. It is well established that density and mechanical properties increase with delivered energy density up to a certain level, above which a slight reduction is seen. Part

density and mechanical properties are thereby directly related to laser fill power and inversely to scan spacing. It is known that the manufactured samples are not isotropic and that part orientation has a great influence on the mechanical properties [20]. However, the effect of these processing parameters on the accuracy of micro-features has been less explored. Furthermore, the established parameter dependencies have not been validated for different manufacturing directions, nor in the context of the mechanical properties of lattice structures. The work presented in this paper quantitatively relates the accuracy and compressive behavior of lattice structures to the process parameters scan spacing, outline laser power and laser fill power. This analysis was examined for the three main manufacturing directions using CCD to explore higher order and interaction effects.

A powder mixture of polycaprolactone (PCL) with 30 wt.% HA was selected for the current experiments. There are conflicting short-term results reported in the literature about the effect of HA addition to PCL composites in terms of cell attachment, proliferation and differentiation. Some authors have discussed how the presence of HA in PCL scaffolds has little or no effect on biological response [20,23-25]. Others showed that scaffolds with 25 wt.% HA demonstrate improved cell differentiation com-pared with PCL scaffolds [26]. Additionally, it has been shown that up to 30 wt.% HA addition improves the mechanical properties of samples by increasing their compressive modulus [27,28]. Therefore, PCL with 30 wt.% HA was selected for this study.

2. Materials and methods

PCL (Sigma Aldrich Chemical Co.) pellets were cryogenically ground and sieved. The powder had an average particle size of 125 μm, with a particle size distribution of 80% of all particles between 70 and 160 μm, as measured with a Malvern Mastersizer particle size analyzer. PCL is a thermoplastic polyester with a melt-ing point of 60 °C and is favorable for SLS processing as it does not decompose below 300 °C [29]. The HA powder used in this experiment was sold under the brand name Captal 60-1 (Plasma Biotal Ltd.) and had an average particle size of 38 μm. A mixture of the PCL and HA powders containing 30 wt.% HA was produced by physical blending and loaded into the feed chambers of the SLS machine.

Test specimens for mechanical testing and accuracy measurements were cubic lattice structures with a relative density of 0.33, strut size of 0.6 mm and pore size length of 1.2 mm. All specimens were designed using SolidWorks® and were exported into STL file format. Fig. 1 shows the designed geometry and the coordinate system used, where layer deposition is in the z-direction.

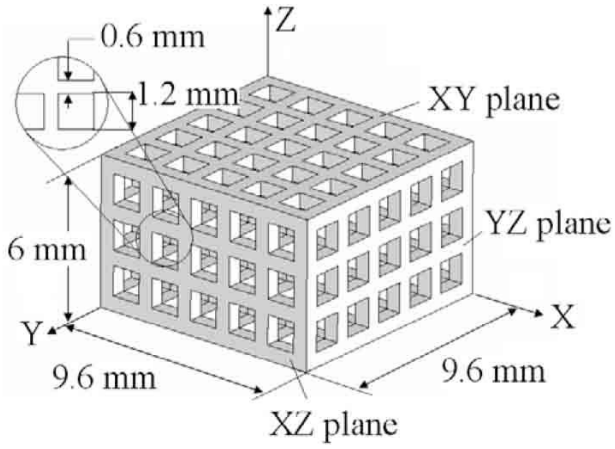

Fig. 1. Cubic lattice structure dimensions and the coordinate system used.

In each build three sets of scaffolds were positioned in such a way that either the scaffold x, y or z axis coincided with the build direction in order to explore issues of anisotropy. A DTM Sinterstation 2500^{Plus} with a 25 W power, continuous wave CO_2 laser focused to a 410 μm spot was used to fabricate the scaffolds. Laser fill power, outline laser power and scan spacing were varied according to the central composite design described below. Laser power is the power at which the fill scan lines are sintered, scan spacing is the distance between two parallel scan lines and outline laser power is the power applied to the contour line of the features (Fig. 2). All other parameters were kept constant: the laser speeds for the outline and fill scans were 1778 and 5080mms^{-1}, respectively, part bed temperature was 38 °C and layer thickness was set to 0.15 mm. Excess powder was brushed off the exterior and the internal architecture was cleaned using compressed air.

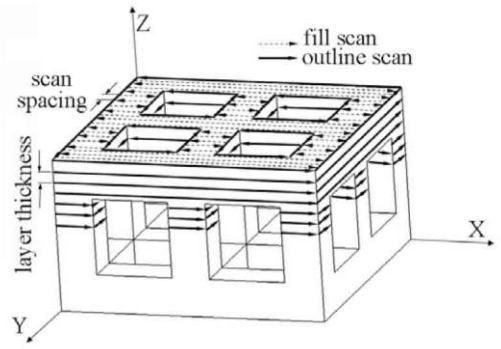

Fig. 2. SLS process parameters and scan patterns in different directions.

A central composite design was applied with four design factors, namely laser fill power (X_1), outline laser power (X_2), scan spacing (X_3) and manufacturing direction (X_4). This design had a core 23 full factorial design, to which the central and axial points were added. The coded levels and the natural values of these factors set in the statistical experiment are shown in Table 1.

Table 1
Coded and natural values of the design factors (the coded values are dimensionless and are shown in bold).

Design factors	**−1.68**	**−1**	**0**	**+1**	**+1.68**
x_1: laser fill power (W)	8.32	9	10	11	11.68
x_2: outline laser power (W)	3.32	4	5	6	6.68
x_3: scan spacing (mm)	0.1	0.12	0.15	0.18	0.2
x_4: building direction		*x*	*y*	*z*	

Six replicates were run at the central point to allow for repeatability analysis and the whole experiment was performed once in the case of mechanical testing and eight times in the case of accuracy analysis. The upper and lower ranges of the process parameters in Table 1 were selected according to the following criteria. When the highest energy density was delivered to the powder bed, i.e. the highest laser fill power of 11.68 W and the smallest scan spacing of 0.1 mm were applied, the powder was visibly strongly melted by the laser beam. In contrast, applying the lowest laser fill power (8.32 W) and the largest scan spacing (0.2 mm) resulted in weakly sintered, fragile structures. As the speed of the outline scan was significantly lower than that of the fill scan, the outline power in the center point of the design space was set to half of the corresponding laser fill power.

The computations were performed with the aid of Design-Ex-pert® software. The corresponding quadratic models for the response functions (accuracy and mechanical properties) were computed using ANOVA. The P value was used as a tool to check the significance of the examined variables. A P value of less than 0.05 (i.e. 95% confidence interval) indicates that the examined parameter is significant. Insignificant effects were determined as those having P values higher than 0.05 and were excluded from the model. Statistics used to determine whether the constructed models were adequate to describe the experimental data were the adequacy of the model ($P < 0.0001$), the lack of fit ($P > 0.1$) test and the signal to noise ratio ($S/N > 7$).

Microscopic images were taken from the surfaces of the scaffolds using a Meiji EMZ-TR optical microscope. Images were analyzed and feature dimensions obtained using Matlab® Image Processing Toolbox.

The compressive mechanical properties of the fabricated specimens were tested according to the ISO 604 standard using a 5 kN load cell at a cross-head speed of 1 mm s^{-1} and with a 1 N preload. A flat plate was used to apply a uniformly distributed load. Compressive modulus, yield strength and yield strain values were obtained using Zwick/Roell Text Expert II software.

3. Results

In the examined range all specimens were successfully fabricated. Fig. 3 shows an SEM (Zeiss EVO LS15) image of the structure of struts fabricated at the center point of the design space. Features designed to be 600 µm were reproduced larger than that. The aver-age width of struts built in the x-direction was 891 µm, for the y-direction struts was 1093 µm and for the z-direction struts was 887 µm. Fig. 4 shows typical images of the parts in the three main building directions and the associated mean dimensions of the features in the center points of the design space.

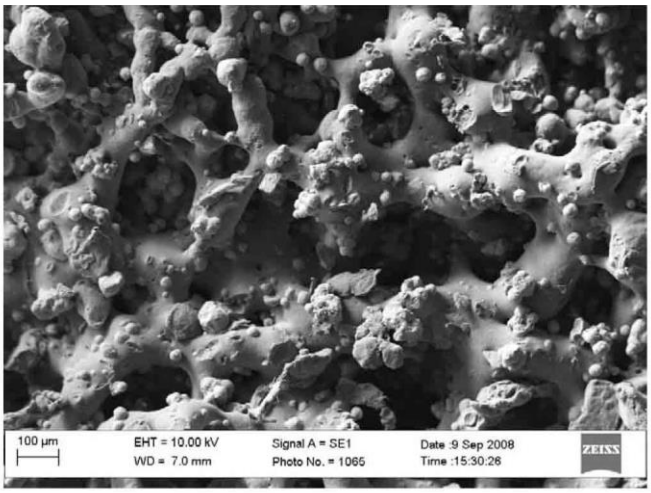

Fig. 3. SEM images of the sintered scaffold surface in the designed solid regions.

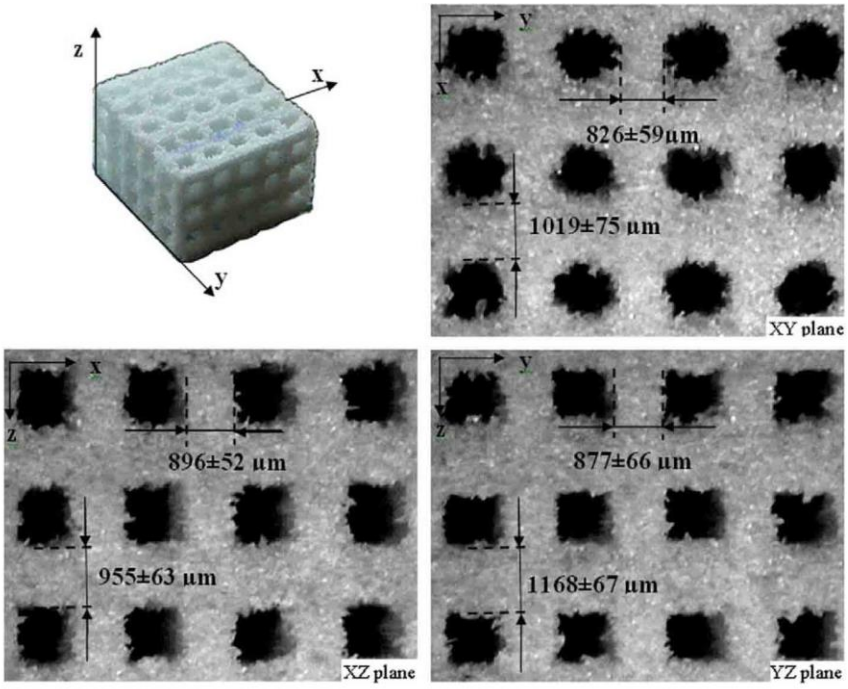

Fig. 4. The surface of fabricated scaffolds in the three principle planes, with strut sizes (average ± standard deviation) measured in the different directions.

The square shape of the pores were reproduced well in the XZ and YZ plane, while in the xy plane the corners of these pores were rounded and therefore had a more circular appearance. A quadratic model was fitted to estimate the linear interaction and quadratic effects of each process parameter on dimensional accuracy. The quadratic model applied to fit the experimental results in each manufacturing direction had the following form:

$$D = b_0 + b_1x_1 + b_2x_2 + b_3x_3 + b_4x_1x_2 + b_4x_1x_2 + b_5x_2x_3 + b_6x_1x_3 + b_7x_1^2, + b_8x_2^2 + b_9x_3^2$$

Where D is the dimension of the feature, x_1 the laser fill power, x_2 the outline laser power and x_3 the scan spacing. Parameters significantly affecting the strut dimensions are listed in Table 2, with the corresponding contribution percentages and P values. Regression coefficients (by) in the different building directions are listed in Table 3.

Table 2
List of contribution percentages and *P* values of significant factors as identified by ANOVA after backward elimination.

Strut	Plane	Factor	Contribution (%)	*P* value
x	*xy*	x_1	5.3	0.0423
		x_2	11.8	0.0104
		x_3	67.8	<0.0001
		x_2x_3	7.5	0.0385
		x_3^2	7.7	0.0245
	xz	x_3	74	<0.0001
		x_3^2	26	<0.0001
y	*xy*	x_1	14.2	0.0021
		x_2	6.7	0.0332
		x_3	62.5	<0.0001
		x_2x_3	12.2	0.0044
		x_3^2	4.3	0.0887
	yz	x_2	6.1	0.370^H
		x_3	3.5	0.495^H
		x_2x_3	35.9	0.0311
		x_3^2	54.4	0.0082
Z	*xz*	x_1	2.4	0.655^H
		x_3	54.3	0.0010
		x_1x_3	11.5	0.0472
		x_3^2	31.8	0.0101
	yz	x_2	46.3	0.0118
		x_3	53.7	0.0068

Terms marked ^{H} are listed to satisfy the hierarchy of the model.

The mechanical behavior of scaffolds fabricated by SLS is not isotropic. When tested under uniaxial compression, scaffolds with load-bearing struts fabricated in the x-direction behaved elastically (Fig. 5), while those fabricated in the y-direction and z-direction behaved more plastically and exhibited a distinct yield point.

Table 3
Regression coefficients of quadratic model terms in the different building and measuring directions.

Strut	Plane	b_0	b_1	b_2	b_3	b_4	b_5	b_6	b_7	b_8	b_9
x	*xy*	62.16	1.488	13.83	−364.8		−77.35				1913.3
	xz	140.8			−609.8						1733.2
y	*xy*	54.78	2.414	16.31	−104.3		−97.68				1413.5
	yz	5.544		7.28	717.0		−51.77				−1568.7
z	*xz*	79.17	6.794		−186.7	−48.72					1977.5
	yz	82.17		−1.16	−41.73						

The elastic modulus was lowest (0.606-1.910 MPa) when compressed struts were fabricated in the x-direction and was the highest (1.95-2.33 MPa) when fabricated in the z-direction. The highest values of yield strength (0.16-0.6 MPa) were observed when compressed struts were built in the y-direction.

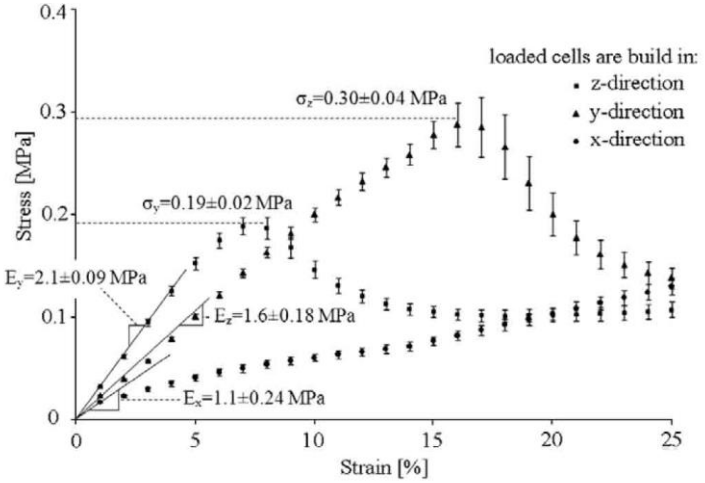

Fig. 5. Compressive behavior of the scaffolds (six replicates in the center points of the design space) in three different building directions.

In terms of compressive modulus, no process parameters have been detected to be significant in the examined parameter range. The direction of loading, however, was identified as significant by ANOVA. Determinative factors of yield strength changed with loading direction. The quadratic models fitted to the experimental data are as follows:

$$\sigma_y = 2.152 + 0.047x_2 - 25.168x_3 + 73.984x_3^2$$

$$\sigma_z = -0.038 + 0.012x_1 + 0.125x_2 - 1.312x_3 - 0.738x_2x_3 + 10.3194x_3^2$$

Specimens that exhibited a yield point showed a strong quadratic dependence on scan spacing (x_3). Furthermore in the y-direction outline laser power (x_2) and in the z-direction the interaction between outline laser power and scan spacing were also significant. The full analysis of variance is presented in Tables 4 and 5.

Table 4
ANOVA table for yield strength of the specimens loaded in the *y* building direction, after backward elimination of the full quadratic model.

Source	Sum of squares	Degrees of freedom	Mean square	*F* value	*P* value
Model	0.204	3	0.068	47.92	<0.0001
x_2	0.031	1	0.031	21.54	0.0003
x_3	0.109	1	0.109	76.46	<0.0001
x_3^2	0.065	1	0.065	45.76	<0.0001
Residual	0.023	16	0.001		
Lack of fit	0.016	11	0.001	1.05	0.5148
Pure error	0.007	5	0.001		

R^2 = 0.9534, adjusted R^2 = 0.9368, predicted R^2 = 0.9076, signal to noise ratio = 25.4.

Table 5
ANOVA table for yield strength of the specimens loaded in the *z* building direction after backward elimination of the full quadratic model.

Source	Sum of squares	Degrees of freedom	Mean square	*F* value	*P* value
Model	0.055	5	0.011	57.32	<0.0001
x_1	0.002	1	0.002	10.12	0.0067
x_2	0.003	1	0.003	15.46	0.0015
x_3	0.045	1	0.044	233.83	<0.0001
$x_2 \times x_3$	0.004	1	0.004	20.55	0.0005
x_3^2	0.001	1	0.001	6.64	0.0219
Residual	0.003	14	0.0001		
Lack of fit	0.001	9	9.42e–05	0.26	0.9620
Pure error	0.0012	5	0.0004		

R^2 = 0.8999, adjusted R^2 = 0.8811, predicted R^2 = 0.8462, signal to noise ratio = 24.8.

4. Discussion

The accuracy of selective laser sintered parts is predominantly determined by powder particle size, focused laser beam diameter and heat transfer in the powder bed [30]. In the present manufacturing process the 125 μm average particle size and 410 μm laser beam spot size are close to the target feature dimension of 600 μm, explaining the low accuracy of the reproduced features. As shown in Fig. 4, the feature shapes were relatively well pre-served in the XZ and YZ planes where accuracy was only affected by the larger particle size of the powder and limited by the set layer thickness. On the other hand, the accuracy of features in the xy plane was affected by the outline scan, where the spot size of the laser had a large influence. The designed square shape (1.2 x 1.2 mm) of the pores was circumscribed by the 410 μm laser spot size, resulting in rounding of the corners of the fabricated pores.

Directional dependence was identified as the predominant factor. Great differences in terms of influential parameters in the three main building directions are the results of varying scan pat-terns, as shown in Fig. 2. Among the processing parameters, scan spacing had a dominant effect in all building directions. Strut thickness was seen to increase quadratically as scan spacing de-creased. Similar findings - an increase in part dimensions with in-creased delivered energy density - were reported by Hao et al. and Caulfield et al. [11,20]. As delivered energy density is determined by scan spacing and laser fill power, it was anticipated that the interaction effect of these two parameters would be significant. This interaction was only significant on strut dimensions fabricated in the z-direction, indicating that the scan spacing range examined had a larger effect than that of the laser power range selected for this work. The applied statistical analysis showed that the fabricated part dimensions are reproducible, therefore, the accuracy of the produced samples should be improved by applying a scaling formula to the designed geometry. Commercial SLS systems enable directional scaling of the parts and also allow for shrinkage and z-growth compensation. However, the laser beam diameter (410 μm) typically used with commercial SLS systems still remains a limiting factor in terms of reproducing micro-features.

The elastic modulus of the scaffolds was mostly dependent on the building direction, resulting from the different scanning pat-terns (see Fig. 2). The parts were weakest in the x-direction, where scan lines were parallel to the loading direction. The highest elastic modulus values were recorded for struts fabricated in the y-direction, where scan lines were perpendicular to loading. No other processing parameters were identified as significant, as a lack of repeatability was experienced in all directions. In order to investigate those parameters affecting the compressive modulus, repeated testing of each point within the design space would initially be required. The investigation of a wider parameter range is also expected, to help the identification and description of the effects of process parameters.

In the x-direction the initial linear elastic regime was followed by a plateau of roughly constant (slightly increasing) stress that was associated with elastic buckling of the load-bearing struts. At large compressive strains strut buckling became the main mechanism and although the deformation was elastic (recoverable), it caused a significant decrease in the load carrying capacity of the structure. Scaffolds fabricated in the other two directions (y and z) showed plastic behavior, exhibiting a distinctive yield point in their stress-strain response after the linear elastic slope. This can be associated with budding of struts and the formation of plastic hinges within the structure. Hinge formation is facilitated by delamination or the shifting of formed layers normal to the loading. It is most prominent in the y-direction, where, after the initial buckling, layers shift on each other and hinges are formed on the load-bearing struts. In the y-direction, although the layers are parallel, the scan lines are perpendicular to the load and hinge formation occurs along these lines. In the case of the x struts both the scan lines and the layers are parallel to the loading, so only buckling is observed. Fig. 6 illustrates these identified failure mechanisms in the three manufacturing directions.

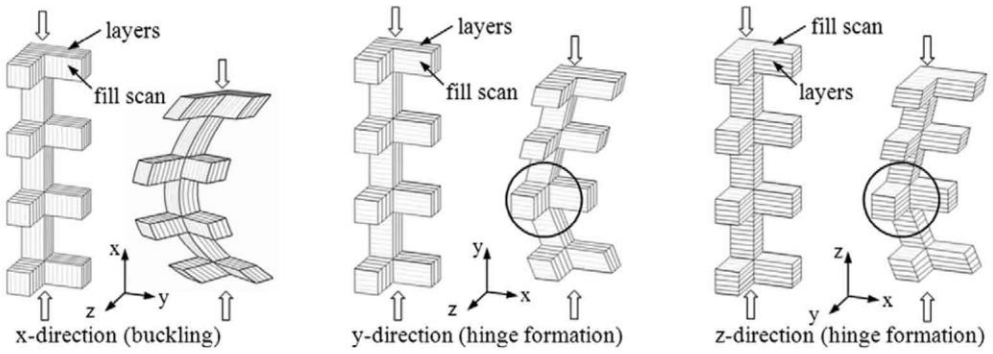

Fig. 6. Scanning patterns of load bearing struts built in various directions and possible failure mechanisms.

Under compression the compressive yield strength of struts fabricated in the y-direction showed an inverse quadratic dependence on scan spacing and directly proportional linear dependence on outline laser power. In the case of z struts the same parameters were significant, with an additional interaction effect between out-line laser power and scan spacing.

For the first time a direct quadratic relationship between scan spacing and strength has been established. This strong influence of scan spacing on mechanical behavior is in agreement with the observations of other groups [19,22,31,32]. The current results also support the findings of Dewidar et al. that parts fabricated at the same energy density level using smaller scan spacing values are denser and, therefore, have superior mechanical properties, suggesting a higher order relationship between scan spacing and mechanical properties [19]. In this CCD scan spacing was varied between 0.1 and 0.2 mm, therefore the degree of scan line overlap changed between approximately 3/4 and 1/2 for the 410 μm spot size. With increased overlapping not only will the delivered energy density increase, but consecutive remelting of the sintered area also changes its reflection and thermal conductivity, resulting in a denser and stronger structure. The inter-action effect noted between scan spacing and outline laser power can also be explained by this phenomenon. If the outline is scanned on the remelted denser area this results in the prevailing mechanical properties. The significance of laser fill power to part density and therefore mechanical properties is well established in the literature [12,18-22,32]. However, it was not seen to be important for accuracy and mechanical properties in the examined range. This lack of significance is possibly due to the selected range of laser fill power or to the fact that the fabricated features in the current experiment were on the micron scale, close to the working diameter of the laser, and therefore outline laser power was more dominant than laser fill power. In this case, for example, it is the outline power that mainly creates a 0.6 mm strut in the xy plane. Compressive properties in the current study (E = 1-2 MPa, σ_y= 0.2-0.6 MPa) are one order of magnitude below the values reported by Williams et al. for the same designed macro-porosity using pure polycaprolactone (E = 16-20 MPa, σ_y = 2-3 MPa) [13]. This significant difference may be due to the differences in the porosity of the designed solid regions. Furthermore, the study presented in this paper intended to fabricate scaffolds with smaller feature sizes, which limited the use of higher energy density levels.

5. Conclusions

Scaffold geometries with a pore size length and strut thickness of —0.9 mm were fabricated with low accuracy. Dimensions in the xz and yz planes were better reproduced than in the xy plane. Of the examined process parameters, manufacturing direction had a predominant effect on both accuracy and mechanical properties. Models have been developed to describe the dependence of yield strength and fabricated dimensions on scan spacing, laser fill power and outline laser power in the three main manufacturing directions. For both response functions a quadratic dependence on scan spacing was identified. The fabricated dimension was directly proportional and yield strength inversely related to scan spacing.

Acknowledgements

This research was een supported by a Marie Curie Early Stage Research Training Fellowship of the European Community's Sixth Framework Programme under contract number MEST-CT-2005- 020621. The authors would like to acknowledge the help of Tamas Szucs in conducting the experiments.

Appendix A. Figures with essential colour discrimination

In this article, Figure 4 is difficult to interpret in black and white. The full colour images can be found in the on-line version, at doi:10.1016/j.actbio.2009.07.018.

References

[1] Nelson JC. Selective laser sintering: a definition of the process and an empirical sintering model. Ph D Dissertation, Faculty of the Graduate School, University of Texas at Austin: Austin, p. 232,1993.

[2] Lorrison J, Dalgarno K, Wood D. Processing of an apatite-mullite glass-ceramic and an hydroxyapatite/phosphate glass composite by selective laser sintering. J Mater Sci: Mater Med 2005;6(8):775-81.

[3] Cruz F, Simoes J, Coole T, Becking C. Direct manufacture of hydroxyapatite based bone implants by selective laser sintering. Virtual Model Rapid Manuf 2005:119.

[4] Wiria FE, Leong KF, Chua CK, Liu Y. Poly-[epsilon]-caprolactone/hydroxyapatite for tissue engineering scaffold fabrication via selective laser sintering. Acta Biomater 2007:3(1):1-12.

[5] Wiria F, Chua C, Leong K, Quah Z, Chandrasekaran M, Lee M. Improved biocomposite development of poly(vinyl alcohol) and hydroxyapatite for tissue engineering scaffold fabrication using selective laser sintering. J Mater Sci: Mater Med 2008;19(3):989-96.

[6] Simpson RL, Wiria FE, Amis AA, Chua CK, Leong KF, Hansen UN, et al. Development of a 95/5 poly (L-lactide-co-glycolide)/hydroxyapatite and beta-tricalcium phosphate scaffold as bone replacement material via selective laser sintering. J Biomed Mater Res B Appl Biomater 2008;84(1):17-25.

[7] Tan KH, Chua CK, Leong KF, Cheah CM, Gui WS, Tan WS, et al. Selective laser sintering of biocompatible polymers for applications in tissue engineering. BioMed Mater Eng 2005;15(1/2):113-24.

[8] Tan KH, Chua CK, Leong KF, Cheah CM, Cheang P, Abu Bakar MS, et al. Scaffold development using selective laser sintering of polyetheretherketone-hydroxyapatite biocomposite blends. Biomaterials 2003;24(18):3115-23.

[9] Tan KH, Chua CK, Leong KF, Naing MW, Cheah CM. Fabrication and characterization of three-dimensional poly(ether-ether-ketone)/ hydroxyapatite biocomposite scaffolds using laser sintering. Proc Inst Mech Eng H: J Eng Med 2005;219(3):183-94.

[10] Savalani MM, Hao L, Zhang Y, Tanner KE, Harris RA. Fabrication of porous bioactive structures using the selective laser sintering technique. Proc Inst Mech Eng H: J Eng Med 2007:873-86.

[11] Hao L, Savalani MM, Zhang Y, Tanner KE, Harris RA. Effects of material morphology and processing conditions on the characteristics of hydroxyapatite and high-density polyethylene biocomposites by selective laser sintering. Proc Inst Mech Eng L: J Mater Design Appl 2006;220(3):125-37.

[12] Hao L, Savalani MM, Zhang Y, Tanner KE, Harris RA. Selective laser sintering of hydroxyapatite reinforced polyethylene composites for bioactive implants and tissue scaffold development. Proc Inst Mech Eng H: J Eng Med 2006;220(4): 521-31.

[13] Williams JM, Adewunmi A, Schek RM, Flanagan CL, Krebsbach PH, Feinberg SJ, et al. Bone tissue engineering using polycaprolactone scaffolds fabricated via selective laser sintering. Biomaterials 2005;26(23):4817-27.

[14] Zhou W, Lee S, Wang M, Cheung W, Ip W. Selective laser sintering of porous tissue engineering scaffolds from poly(L-lactide)/carbonated hydroxyapatite nanocomposite microspheres. J Mater Sci: Mater Med 2008;19(7):2535-40.

[15] Partee B, Hollister SJ, Das S. Selective laser sintering process optimization for layered manufacturing of CAPA® 6501 polycaprolactone bone tissue engineering scaffolds. J Manuf Sci Eng 2006;128(2):531-40.

[16] Evans M. Optimisation of manufacturing processes - a response surface approach. London: Maney Publishing; 2003.

[17] Montgomery DC, Runger GC, Hubele NF. Engineering statistics. Hoboken, NJ: John Wiley and Sons Inc.; 2001.

[18] Ho HCH, Gibson I, Cheung WL. Effects of energy density on morphology and properties of selective laser sintered polycarbonate. J Mater Process Technol 1999;89-90:204-10.

[19] Dewidar MM, Dalgarno KW, Wright CS. Processing conditions and mechanical properties of high-speed steel parts fabricated using direct selective laser sintering. Proc lnst Mech Eng B Eng Manuf 2003:1651-63.

[20] Caulfield B, McHugh PE, Lohfeld S. Dependence of mechanical properties of polyamide components on build parameters in the SLS process. J Mater Process Technol 2007;182(1-3):477-88.

[21] Leong K, Phua KK, Chua C, Du Z, Teo KO. Fabrication of porous polymeric matrix drug delivery devices using the selective laser sintering technique. Proc Inst Mech Eng H: J Eng Med 2001;215(2):191-2.

[22] Simchi A, Pohl H. Effects of laser sintering processing parameters on the microstructure and densification of iron powder. Mater Sci Eng A 2003; 359(1-2):119-28.

[23] Vincenzo Guarino FC, Netti PA, Ciapetti G, Pagani S, Martini D, Baldini N, et al. The role of hydroxyapatite as solid signal on performance of PCL porous scaffolds for bone tissue regeneration. J Biomed Mater Res B: Appl Biomater 2008;86B(2):548-57.

[24] Endres M, Hutmacher D, Salgado A, Kaps C, Ringe J, Reis R, et al. Osteogenic induction of human bone marrow-derived mesenchymal progenitor cells in novel synthetic polymer-hydrogel matrices. Tissue Eng 2003;9(4):689-702.

[25] Chim H, Hutmacher DW, Chou AM, Oliveira AL, Reis RL, Lim TC, et al. A comparative analysis of scaffold material modifications for load-bearing applications in bone tissue engineering. Int J Oral Maxillofacial Surg 2006;35(10):928-34.

[26] Shor L, Giiceri S, Wen X, Gandhi M, Sun W. Fabrication of three-dimensional polycaprolactone/hydroxyapatite tissue scaffolds and osteoblast-scaffold interactions in vitro. Biomaterials 2007;28(35):5291-7.

[27] Eosoly S, Lohfeld S, Brabazon D. Effect of hydroxyapatite on biodegradable scaffolds fabricated by SLS. Key Eng Mater 2009;396-398:659-62.

[28] Azevedo M, Reis R, Claase M, Grijpma D, Feijen J. Development and properties of polycaprolactone/hydroxyapatite composite biomaterials. J Mater Sci: Mater Med 2003;14(2):103-7.

[29] Kweon H, Yoo MK, Park 1K, Kim TH, Lee HC, Lee H-S, et al. A novel degradable polycaprolactone network for tissue engineering. Biomaterials 2003;24(5): 801-8.

[30] Shi Y, Li Z, Huang S, Zeng F. Effect of the properties of the polymer materials on the quality of selective laser sintering parts. Proc Inst Mech Eng L: J Mater Design Appl 2004;218(3):247-52.

[31] Chatterjee AN, Kumar S, Saha P, Mishra PK, Choudhury R. An experimental design approach to selective laser sintering of low carbon steel. J Mater Process Technol 2003;136:151-7.

[32] Gibson I, Shi D. Material properties and fabrication parameters in selective laser sintering. Rapid Prototyping J 1997;3(4):129-36.